arXiv:1511.05508v1 [quant-ph] 17 Nov 2015

New insights into mode behaviours in waveguides with impedance boundary conditions

WenPing Bi, Vincent Pagneux

November 18, 2015

Laboratoire d'Acoustique de l'Université du Maine,
UMR CNRS 6613
Av. O Messiaen, 72085 LE MANS Cedex 9,
France

Abstract

In this paper we investigate mode nonorthogonal properties and their effects on the sound power attenuation in a waveguide with impedance boundary conditions. By introducing two quantities: self-nonorthogonality K_p, which measures the nonorthogonality between left and right eigenfunctions of a mode, and mutual-nonorthogonality S_{ij}, which measures the nonorthogonality between modes i and j, two opposite limiting cases are clearly identified in the boundary impedance $\mathbb{Z}$ plane: one is non-dissipation, i.e., acoustic rigid, pressure-release, and purely reactive impedance; the other is Cremer's optimum impedances which are exceptional points — a subject has attracted much attention in recent years in different physical domains. Variations along an arbitrary path in the complex boundary impedance plane, K_p and $S_{i,j}$ varies between the two opposite extremes. It is found that K_p and $S_{i,j}$ play crucial roles in sound power attenuation.

1 Introduction

Modes in an infinite Waveguide with Impedance Boundary Conditions (WIBC) are a basic concept in acoustic textbooks, such as Refs. [1] and [2], and a powerful tool to understand the complex sound field in applications, such as ducts lined with locally-reacting acoustically absorbent materials, for review articles in aircraft engine duct systems see, for example, Refs. [3] and the references therein. Mode method in a WIBC has been the subject of much research for more than 50 years. It is remarkable that there remain fundamental open questions; e.g., how to measure the nonorthogonality between modes when the boundary impedance is complex, and what are their effects on sound power attenuation?

Another fundamental problem which is not full understood is the Cremer's optimum impedance. The optimization defined by Cremer[4] is relative to the

modal axial sound attenuation rates in an infinite WIBC. The maximum sound attenuation rate of individual mode is achieved by choosing the corresponding optimum wall impedance. Cremer[4] investigated only the least attenuation mode. Tester[5] generalised this concept to arbitrary higher order modes. Cremer's optimum impedance has been one of the most important liner design method[5, 7, 8, 9, 6, 14, 10, 11, 12, 13, 15, 16, 17, 18]. Its optimum condition leads to double eigenvalues of the dispersion equation. These double eigenvalues of dispersion equation have been inquired by Morse[19], and studied by Tester[5], Zorumski[6], Mechel [8, 9], and Shendrov[20]. They form square-root branch points in the complex admittance plane[5, 8, 9]. However, nothing is known about the eigenfunction behaviors in the vicinity of the branch points or optimum impedances up to now.

Due to the nonorthogonality, total sound power is no longer the sum of sound power in individual modes, when multimodes propagate in a WIBC. Cross-powers make contribution to the total sound power. Creamer's optimum impedance aimes only at the maximum attenuation of individual mode. No attempt has been made to investigate the cross-power. Little was known about what are the effects of source and impedance boundary conditions on the cross-power propagations.

In this paper, we study mode nonorthogonal properties and their effects on the sound power attenuation in a WIBC. The paper is organised as follows. In Sec. 2, we show that Cremer's optimum impedances are exceptional points, at which not only eigenvalues but also the associated eigenfunctions coalesce, the left eigenfunctions and right eigenfunctions of the coalescent modes are orthogonal. We introduce two physical quantities: self-nonorthogonality K_p, to measure the nonorthogonality between left and right eigenfunctions of individual mode; and mutual-nonorthogonality S_{ij}, to measure the nonorthogonality between modes i and j. Two opposite limiting cases: $K_p = 1$, $S_{ij} = 0$ and $K_p = \infty$, $S_{i,j} = 1$ are clearly identified in the whole complex boundary impedance $\mathbb{Z}$ plane, correspond to: non-dissipation, i.e., acoustic rigid, pressure-release, and purely reactive impedance, and the Cremer's optimum impedances, respectively. Variations along an arbitrary path in the complex boundary impedance plane, K_p varies between 1 and ∞, and $S_{i,j}$ varies between 0 and 1. The roles of K_p and S_{ij} in sound power attenuation in a semi-infinite WIBC are illustrated in Sec. 3.

The model of the present paper is chosen to be a cylindrical waveguide with circular cross-section. Such model is the most common in practical applications. The extensions to rectangular or annular waveguides are straightforward. Flow effects will be considered in the further work.

2 Mode behaviors

We consider an infinite long cylindrical waveguide, of uniform and circular cross section, having locally reactive impedance wall boundary conditions. The impedance is assumed uniform along axial and circumferential directions, respectively. Linear and lossless sound propagation in air is assumed. With time dependence $\exp(j\omega t)$ omitted, the eigenvalues γ and eigenfunctions $\tilde{\phi}$ of modes satisfies the Laplacian

eigenvalue problem

$$\nabla_\perp^2 \tilde{\phi}_{mn} = -\gamma_{mn}^2 \tilde{\phi}_{mn}, \tag{1}$$

where

$$\nabla_\perp^2 = \frac{1}{r}\frac{\partial}{\partial r}(r\frac{\partial}{\partial r}) + \frac{1}{r^2}\frac{\partial^2}{\partial \theta^2},$$

with the boundary condition

$$\frac{\partial \tilde{\phi}_{mn}}{\partial r} = Y\tilde{\phi}_{mn}, \text{ at } r = 1, \tag{2}$$

where m and n refer to, respectively, the circumferential and radial mode indices. $Y = -jK\beta_0$. $\beta_0 = 1/Z_0$, where Z_0 and β_0 are wall boundary impedance and admittance, respectively. They are complex number. $K = \omega R/c_0$ refers to the dimensionless frequency, R is the radius of the waveguide. By assuming the solution

$$\tilde{\phi}_{mn}(r,\theta) = \frac{J_m(\gamma_{mn}r)}{J_m(\gamma_{mn})} \begin{cases} \cos(m\theta) \\ \sin(m\theta), \end{cases} \tag{3}$$

we obtain the dispersion equation for the eigenvalues

$$\gamma_{mn}\frac{J_m'(\gamma_{mn})}{J_m(\gamma_{mn})} = Y. \tag{4}$$

If we define an operator $\mathscr{L} = \nabla_\perp^2 + \gamma_{mn}^2$, the eigenvalue problem defined by Eqs. (1) and (2) can be rewritten as

$$\mathscr{L}\tilde{\phi}_{mn} = 0, \tag{5}$$

with the boundary condution

$$\mathscr{G}\tilde{\phi}_{mn} = 0, \text{ at } r = 1, \tag{6}$$

where $\mathscr{G} = \partial/\partial r - Y$. We introduce a function $\tilde{\varphi}$ to define the adjoint eigenvalue problem (see appendix A)

$$\mathscr{L}^+\tilde{\varphi}_{mn} = 0, \ \ \mathscr{G}^+\tilde{\varphi}_{mn} = 0 \text{ at } r = 1, \tag{7}$$

where $\mathscr{L}^+ = \nabla_\perp^2 + (\gamma_{mn}^2)^*$, $\mathscr{G}^+ = \partial/\partial r - Y^*$.

We will call $\tilde{\phi}_{mn}$ right eigenfunctions and $\tilde{\varphi}_{mn}$ left eigenfunctions in the following sections.

2.1 Basic behaviors

When the boundary is acoustically rigid ($\beta_0 = 0$), pressure release ($\beta_0 = \infty$), or purely reactive without dissipation ($\beta_0 = jc$, c is real), the eigenvalue problems defined by Eqs. (1) and (2) or (5) and (6) are self-adjoint (see Appendix A), i.e.,

$\mathscr{L}^+ = \mathscr{L}$ and $\mathscr{G}^+ = \mathscr{G}$. Therefore, $\tilde{\phi}_{mn} = \tilde{\varphi}_{mn}$. The eigenfunctions $\tilde{\phi}_{mn}$ form a complete set of function and are mutual-orthogonal in the sense

$$\int_s \tilde{\phi}_{mn}\tilde{\phi}^*_{m'n'}ds = \Lambda_{mn}\delta_{mm'}\delta_{nn'}, \tag{8}$$

where "*" refers to complex conjugate, Λ_{mn} are normalized constants, δ is Kronecker delta function, s is the cross section of waveguides.

On the other hand, when the wall impedance is complex, i.e., dissipation is included, the eigenvalue problems defined in Eqs. (1) and (2) or (5) and (6) are not self-adjoint (see Appendix A). However, it can be proved (see Appendix A) that the eigenfunctions $\tilde{\phi}_{mn}$ and their adjoint $\tilde{\varphi}_{mn}$ are orthogonal

$$\int_s \tilde{\phi}_{mn}\tilde{\varphi}^*_{m'n'}ds = \Lambda'_{mn}\delta_{mm'}\delta_{nn'}. \tag{9}$$

This means that the eigenfunctions $\tilde{\phi}_{mn}$ ($\tilde{\varphi}_{mn}$) are not mutual-orthogonal, $\int_s \tilde{\phi}_{mn}\tilde{\phi}^*_{m'n'}ds \neq 0$, when $m \neq m', n \neq n'$, but bi-orthogonal,

$$\int_s \tilde{\phi}_{mn}\tilde{\phi}_{m'n'}ds = \Lambda'_{mn}\delta_{mm'}\delta_{nn'}, \tag{10}$$

where we have used $\tilde{\phi}_{mn} = \tilde{\varphi}^*_{mn}$ (see Appendix A). It is noted that there is no complex conjugate operation on the eigenfunctions $\tilde{\phi}_{m'n'}$.

Wether the eigenfunctions are orthogonal or bi-orthogonal, in this paper, the eigenfunctions $\tilde{\phi}_{mn}$ and $\tilde{\varphi}_{mn}$ are normalized as

$$\phi_{mn}(r,\theta) = \frac{1}{\sqrt{\Lambda_{mn}}}\tilde{\phi}_{mn}(r,\theta), \quad \varphi_{mn}(r,\theta) = \frac{1}{\sqrt{\Lambda_{mn}}}\tilde{\varphi}_{mn}(r,\theta) \tag{11}$$

where Λ_{mn} are defined in Eq. (8).

There are an infinite number of modes in a WIBC corresponding to $m = 0 - \infty$ and $n = 0 - \infty$. They can be classified in two categories[8, 9, 21]: guided modes resulting from the finiteness of the waveguide geometry, and surface modes that exist only near the cavity wall and decay exponentially away from the wall. Typical eigenvalue distributions are shown in Fig. 1 for $m = 0$ and Fig. 2 for $|m| = 0 - 30$, when $K = 30$, $\beta_0 = 0.4 + 0.2j$ which are typical industrial values in the lined intakes of an aeroengine. There is only one surface mode when $m = 0$ as shown in Fig. 1. There are an infinite number of discrete surface modes in a WIBC corresponding to $m = 0 - \infty$, as shown in Fig. 2(a) by "$\oplus$". For each azimuthal order $|m|$ (except $m = 0$), there are only two ($+|m|$ and $-|m|$) surface modes which are in degeneracy. It is noted that this degeneracy is totally different from the branch points and exceptional points in the following sections. In Fig. 2 (a), each $\oplus$ corresponds to one $|m|$. They are arranged as $m = 0, \ \pm 1, \ \pm 2, \ \cdots$, from left to right. The decaying rates of the surface mode amplitudes away from the wall are decided by the imaginary parts of the surface mode eigenvalues γ_m. A typical surface mode profile corresponding to $m = 2$ is shown in Fig. 2(c) and (d).

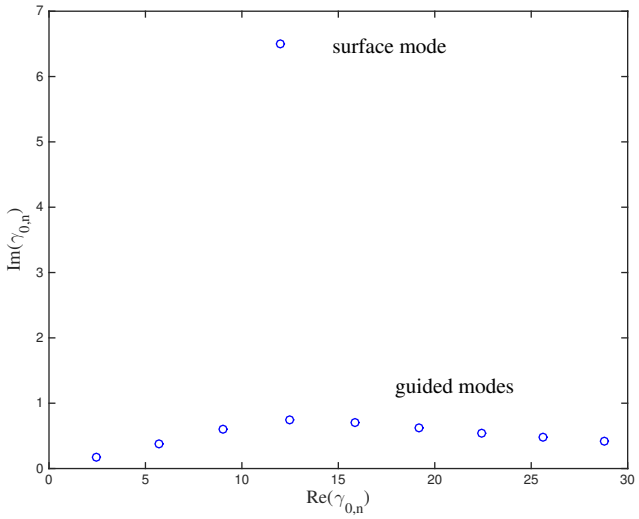

Figure 1: (Color online) Typical eigenvalues in a waveguide with impedance boundary conditions, $K = 30$, $\beta_0 = 0.4 + 0.2j$, $m = 0$.

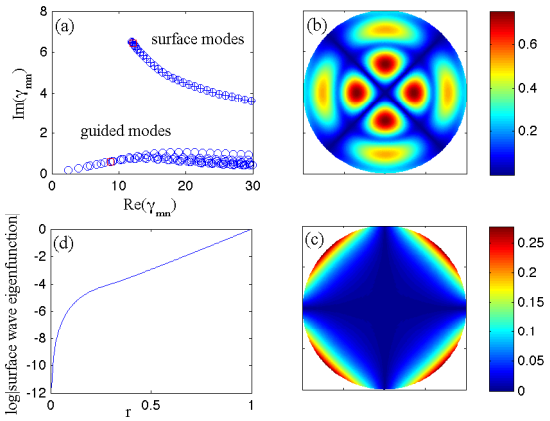

Figure 2: (Color online) Eigenvalues and eigenfunctions of a WIBC, $K = 30$, $\beta_0 = 0.4 + 0.2j$, $|m| = 0 - 30$. (a) eigenvalues, $\oplus$ refers to surface modes (eigenvalues corresponding to $\mathrm{Im}(\gamma_{mn}) > 3$ in this figure), (b) eigenfunction (not normalized) of guided mode (2,1), whose eigenvalue is shown as $\square$ in the branch of guided modes in (a), (c) eigenfunction (not normalized) of surface mode $m = 2$, whose eigenvalue is shown as $\square$ in the branch of surface modes in (a), (d) the eigenfunction profile along r of surface mode $m = 2$.

It needs to stress that the surface modes in a WIBC are asymptotic solutions in high frequency ω. The eigenfunctions become exponentially decaying along r like $e^{\omega|\Im m(\gamma)|(1-r)}/\sqrt{r}$,[21] where $\Im$m refers to the imaginary part. Strictly speaking, they should be called "quasi-surface modes". The eigenvalues of guided modes

are marked by "o" in Fig. 2(a). The eigenfunction of guided mode $(2,1)$, as an example, is plotted in Fig. 2(b).

Because the waveguide is circumferentially uniform. Modes among different azimuthal order m are not coupled. In the following sections, we illustrate the results only for $m = 0$. It is straightforward to extend the results to $m \neq 0$. The index $m = 0$ is then omitted. Without loss of generality, we set $K = 30$.

2.2 Cremer's optimum impedance, branch points, and exceptional pointes

Creamer's optimum impedance in an infinite WIBC has important applications in liner design to reduce noise in industry ducts. The optimization defined by Cremer is relative to the modal axial sound attenuation rates. The maximum sound attenuation rate of each mode is achieved by choosing the corresponding optimum wall impedance. Cremer's optimum condition leads to double eigenvalues of the dispersion equation as defined in Eqs. (43). In the vicinity of the Creamer's optimum impedance, the eigenvalues, which have no power series expansion, are expressed approximately to the lowest order as[5] (see Appendix B)

$$\gamma_n - \gamma_{\text{cremer}} \approx -\sqrt{\frac{2\partial f/\partial \beta_0}{\partial^2 f/\partial \gamma_n^2}}\sqrt{\beta_0 - \beta_{\text{cremer}}}, \tag{12}$$

where we have assumed that the dispersion equation (4) has no triple or higher order eigenvalues, β_{cremer} refers to the admittance at Cremer's optimum impedance. Mathematically, Eq. (12) clearly shows that Creamer's optimum impedance is a branch point in complex boundary impedance plane.

The branch point behaviour can be proved to be a physical reality by an experiment. A numerical simulation is shown In Fig.3. We plot the variations of the real and imaginary parts of eigenvalues as a function of $\Re e(\beta_0)$ when $\Im m(\beta_0) = 0.042655$ ((a), (b)), and $\Im m(\beta_0) = 0.042652$ ((c), (d)) in the vicinity of the first Creamer's optimum impedance $\beta_{\text{cremer}} = 0.099346 + 0.042653j$. The cusp (in Fig. 3 (b), (c)) originated from the square root behavior of the singularity is clearly seen. To illustrate the square root branch point singularity, we numerically encircle the Creamer's optimum impedance in the complex admittance plane in a complete loop: $(\Re e(\beta_0), \Im m(\beta_0)) = (0.095, 0.042655) - (0.105, 0.042655) - (0.105, 0.042652) - (0.095, 0.042652) - (0.095, 0.042655)$. In this loop, the eigenvalues depend only weakly on $\Im m(\beta_0)$, we do not present the results for the varying $\Im m(\beta_0)$. After β_{cremer} is encircled the complex eigenvalues are interchanged. It means that a full loop in the eigenvalue plane requires two loops in the complex admittance plane. A real experiment can re-produce the above process except that β_0 and γ are less accurate. It is noted that the square root branch point behaviour has been experimentally observed by Dembowski *et al*[22] in a microwave cavity with dissipation, recently.

At the Creamer's optimum impedance, not only the eigenvalues of a pair of neighbour modes, but also the corresponding eigenfunctions coalesce. This can

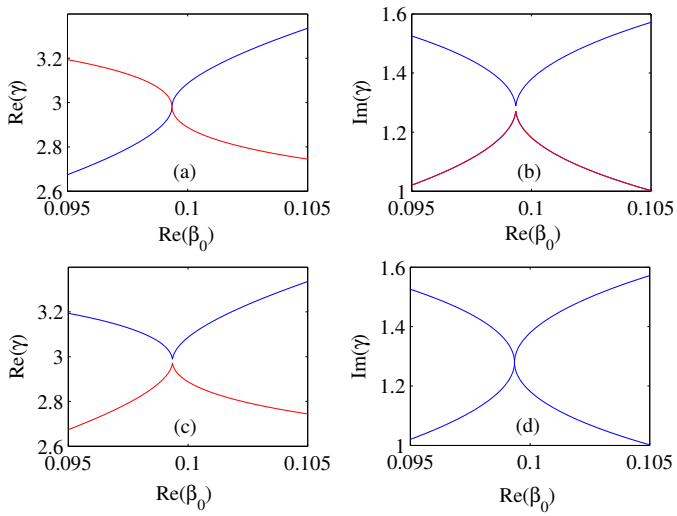

Figure 3: (Color online) Real and imaginary parts of eigenvalue trajectories of modes $n = 0$ and $n = 1$ in the vicinity of the first Cremer's optimum impedance as a function of $\Re e(\beta_0)$, $m = 0$. $\beta_{\text{cremer}} = 0.099346 + 0.042653j$. (a) and (b), $\Im m(\beta_0) = 0.042655$; (c) and (d), $\Im m(\beta_0) = 0.042652$.

be illustrated by calculating the mutual-overlap integral for the mode pair n and $n+1$ in the vicinity of Creamer's optimum impedance,

$$\int_s \phi_n(r,\theta)\phi^*_{n+1}(r,\theta)ds = \int_s \frac{1}{\sqrt{\Lambda_n}}\tilde{\phi}_n(r,\theta)\frac{1}{\sqrt{\Lambda_{n+1}}}\tilde{\phi}^*_{n+1}(r,\theta)ds \qquad (13)$$
$$= \frac{\int_s \tilde{\phi}_n\tilde{\phi}^*_{n+1}ds}{\sqrt{\int_s \tilde{\phi}_n\tilde{\phi}^*_n ds \int_s \tilde{\phi}_{n+1}\tilde{\phi}^*_{n+1}ds}},$$

where we have used Eq. (11). In Fig. 4, we plot variations of the mutual-overlap integral of mode pair $n = 0$ and $n = 1$ as a function of $\Im m(\beta_0)$. The mutual-overlap integral is equal to 1 at $\beta_{\text{cremer}} = 0.099346 + 0.042653j$.

It can be further shown that at the Creamer's optimum impedance, the left and right eigenfunctions of the coalescent modes are orthogonal (self-orthogonality). This can be illustrated by calculating the self-overlap integral of the left and right eigenfunctions

$$\int_s \phi_n(r,\theta)\varphi^*_n(r,\theta)ds = \int_s \frac{1}{\sqrt{\Lambda_n}}\tilde{\phi}_n(r,\theta)\frac{1}{\sqrt{\Lambda_n}}\tilde{\varphi}^*_n(r,\theta)ds \qquad (14)$$
$$= \frac{\int_s \tilde{\phi}_n\tilde{\varphi}^*_n ds}{\int_s \tilde{\phi}_n\tilde{\phi}^*_n ds}.$$

as a function of $\Im m(\beta_0)$ for mode n in the vicinity of Creamer's optimum

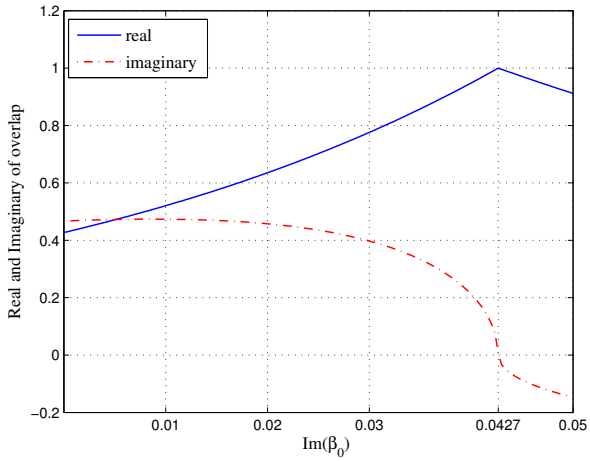

Figure 4: (Color online) Mutual-overlap integral Eq. (13) of the eigenfunctions of mode pair $n = 0$ and $n = 1$ as a function of $\Im m(\beta_0)$, when $\Re e(\beta_0 = 0.099)$. $m = 0$. Solid line, real part, dashed line, imaginary part. At Cremer's optimum impedance $\beta_{\text{creamer}} = 0.099346 + 0.042653j$, the overlap integral is equal to 1.

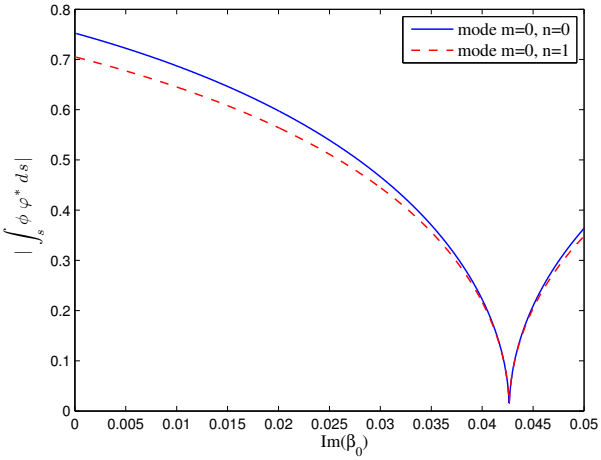

Figure 5: (Color online) Absolute value of the self-overlap integral Eq. (14) of the left and right eigenfunctions of modes $n = 0$ and $n = 1$ as a function of $\Im m(\beta_0)$, when $\Re e(\beta_0 = 0.099)$. Solid line, mode $n = 0$, dashed line, mode $n = 1$. $m = 0$. At Cremer's optimum impedance $\beta_{\text{creamer}} = 0.099346 + 0.042653j$, the self-overlap integral is equal to 0.

impedance. In Fig.5, we plot variations of the absolute value of the self-overlap integral for modes $n = 0$ and $n = 1$. At the Cremer's optimum impedance $\beta_{\text{cremer}} = 0.099346 + 0.042653j$, the self-overlap integral is equal to 0.

The point in a complex plane at which both eigenvalues and the corresponding

eigenfunctions coalesce is called exceptional point (EP). EP should not be confused with a degeneracy, as mentioned above for the surface modes of $+|m|$ and $-|m|$, at which the corresponding eigenfunctions are still orthogonal. Recently, EPs have attracted much attention. The important properties of EPs have been uncovered by Heiss[23, 24, 26, 25], Rotter[27], and Berry[28] for physical systems with dissipation or non-Hermitian system. EPs have been found in different systems, such as, laser-induced ionization states of atoms [29], electronic circuits [30], atoms in cross magnetic and electric fields [31], a chaotic optical microcavity[32], and $\mathscr{P}\mathscr{T}$-symmetric waveguides[33]. This is the first time that EPs and their effects are illustrated in acoustics, to the best of the authors' knowledge.

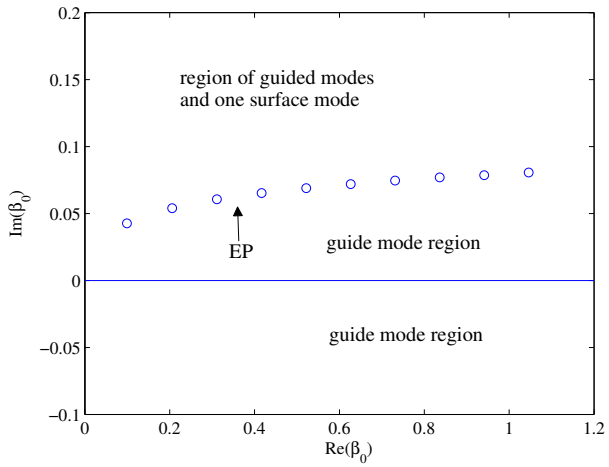

Figure 6: (Color online) Distribution of the first 10 EPs in the complex admittance plane, when $m = 0$.

There are an infinite number of EPs in the complex admittance plane for each circumferenial index m. They can be calculated by Eq. (43) (see Ref. [9], for example). The first 10 EPs when $m = 0$ are illustrated in Fig. 6. The EPs separate the complex admittance plane into two regions: in the lower region, there exist only guided modes, whereas in the upper region, there exist guided modes and one surface mode (for each m). The surface modes take place only in the $\Im m(\beta_0) > 0$ plane (convention $e^{j\omega t}$ is used).

To finish this section, we would like to point out that the mechanism of Creamer's optimum impedance is not explained to date. As was pointed by Tester[5] in 1973 that "A most intriguing property of theoretical and experimental decay rates of modes in lined ducts, for which there is no obvious explanation, is the existence of maximum decay rates for values of the liner impedance which, at first sight, are arbitrary and totally unconnected with any simple results associated with absorption by reflecting boundaries.". This mechanism will be explained in Ref. [34].

2.3 EPs, avoided crossings, and mode localisation

Avoided crossings occur in the vicinity of an EP. This can be illustrated by a 2×2 non-Hermitian matrix

$$\mathsf{H} = \begin{pmatrix} \alpha_1 & 0 \\ 0 & \alpha_2 \end{pmatrix} + \lambda \begin{pmatrix} 0 & c \\ c & 0 \end{pmatrix}, \tag{15}$$

where all the elements are complex. A corresponding physical problem can be

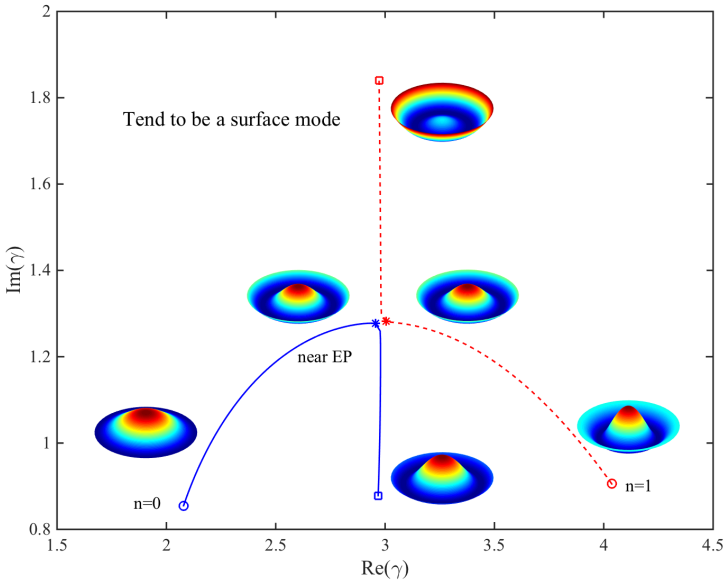

Figure 7: (Color online) Eigenvalue trajectories passing near the first EP as a function of $\Im m(\beta_0)$. $\Re e(\beta_0) = 0.09935 > \Re e(\beta_{\rm EP})$. $\Im m(\beta_0) = 0 - 0.05$. '$\circ$', $\Im m(\beta_0) = 0$; '$\square$', $\Im m(\beta_0) = 0.05$; and '$*$' refers to near $\Im m(\beta_{\rm EP})$. $m = 0$.

found in Ref. [34]. The eigenvalues of H are

$$\gamma_{1,2} = \frac{1}{2}(\alpha_1 + \alpha_2 \pm R), \quad R = \sqrt{(\alpha_1 - \alpha_2)^2 + 4\lambda^2 c^2}). \tag{16}$$

At the EPs, $\lambda_{\rm EPs} = \pm(\alpha_1 - \alpha_2)/(2c)$, $R = 0$, the two eigenvalues coalesce $\gamma_{1,2} = \frac{1}{2}(\alpha_1 + \alpha_2)$, the corresponding eigenvectors also coalesce $\mathbf{x}_{1,2} = C[1, j]$ or $\mathbf{x}_{1,2} = C[1, -j]$. When $R \neq 0$, the eigenvalues avoided crossing as a function of λ. Avoided crossings of eigenvalues have been found in the area of structural dynamics[35, 36, 37, 38] and related to mode localisation in disordered structures[39, 40, 41].

The eigenvalue trajectories in the vicinity of the first EP ($\beta_{\rm BP} = 0.099346 + 0.042653j$) is shown in Fig. 7 as a function of $\Im m(\beta_0)$, when $\Re e(\beta_0) = 0.09935 > \Re e(\beta_{\rm EP})$ is fixed. The eigenfunctions at some selected β_0 are also plotted. As $\Im m(\beta_0)$ increase, the imaginary parts of the eigenvalues of mode $n = 0$ and those

of mode $n = 1$ increase until β_0 approaches the EP, where the eigenvalues form an avoided crossing and the eigenfunctions mix strongly. With a further increase of $\Im m(\beta_0)$, mode $n = 1$ turns to be a surface mode which is localized near the guide wall as mentioned in section 2.1, and mode $n = 0$ turn to a mode which resembles mode $n = 1$. The modes exhibit a similar behavior as we plot the eigenvalue trajectories as a function of $\Im m(\beta_0)$, when $\Re e(\beta_0) = 0.09933 < \Re e(\beta_{\rm EP})$ is fixed. The only difference is that it is mode $n = 0$ turn to be a surface mode and mode $n = 1$ return to a mode which resembles mode $n = 1$.

It needs to stress that the mode localisation mentioned above is explained as a "resonance trapping" effect[34], and is different from these studied in Ref. [39, 40, 41] which are due to disorder effects.

2.4 Riemann surfaces

Another way to illustrate the structures of eigenvalues in the vicinities of EPs and the connections between EPs and avoided crossings is to plot the Riemann surface of eigenvalues over β_0 surface as shown in Figs. 8 and 9 for the first three modes. The values at the first two EPs $\gamma_{\rm EP1}$ and $\gamma_{\rm EP2}$ are pointed out in the figures. Modes with higher circumferential modal order ($m > 1$) or higher radial mode order ($n \geq 2$) exhibit similar characteristics.

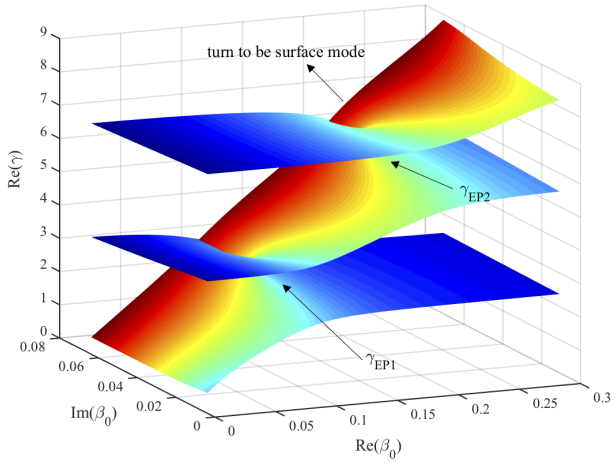

Figure 8: (Color online) Riemann surfaces of the eigenvalues as a function of admittance β_0. Real part of the eigenvalues. The first two EPs are shown. $m = 0$.

It is well known that mode eigenvalues can vary continuously from one mode to another with continuous varying impedance. This can also be seen from the Riemann surfaces in Figs. 8 and 9. The branch cuts separating one mode from another is arbitrary. When surface modes are present, it is not easy to find unambiguous branch cuts to distinguish the modes. In this paper, we define the

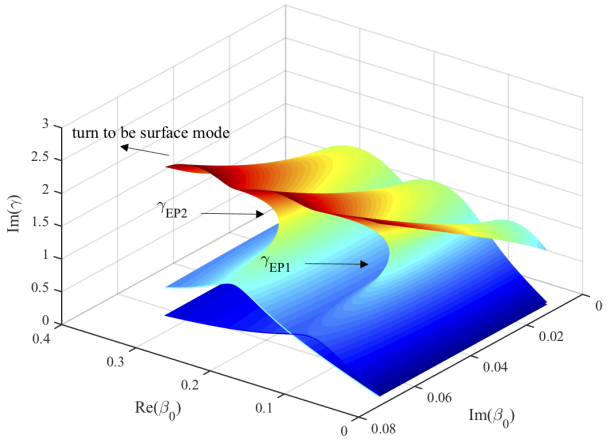

Figure 9: (Color online) Riemann surfaces of the eigenvalues as functions of admittance β_0. Imaginary part of the eigenvalues. The first two EPs are shown. It is noted that to see more clearly the structures of the Riemann surfaces, the imaginary parts are shown in different viewpoint. $m = 0$.

mode index $n = 0,\ 1, \cdots$, according to the ascending order of the real parts of eigenvalues.

2.5 Self-nonorthogonality K_p and mutual-nonorthogonality S_{ij}

Inspired by the coalescence of eigenfunctions between two neighbour modes and orthogonality between left and right eigenfunctions of the coalescent modes at an EP, we define two quantities: self-nonorthogonality $K_{p,n}$ and mutual-nonorthogonality S_{ij}

$$K'_{p,n} = \frac{\sqrt{\int_s \tilde{\phi}_n \tilde{\phi}_n^* ds \int_s \tilde{\varphi}_n \tilde{\varphi}_n^* ds}}{\int_s \tilde{\phi}_n \tilde{\varphi}_n^* ds}, \quad K_{p,n} = K'_{p,n} * (K'_{p,n})^*, \tag{17}$$

$$S_{ij} = \frac{\int_s \tilde{\phi}_i \tilde{\phi}_j^* ds}{\sqrt{\int_s \tilde{\phi}_i \tilde{\phi}_i^* ds \int_s \tilde{\phi}_j \tilde{\phi}_j^* ds}} = \int_s \phi_i(r,\theta)\phi_j^*(r,\theta) ds, \tag{18}$$

to measure the nonorthogonality between left and right eigenfunctions of individual mode n and nonorthogonality between modes i and j in the whole complex impedance (admittance) plane, respectively. It is noted that K_p has been proposed by Petermann[42] for explaining the discrepancy between the theoretically expected natural line-width using the Schawlow-Townes formula and the experimental measured enhanced line-width of a gain-guided single mode semiconductor laser.

Two opposite limiting cases can be identified in the complex β_0 plane:

Case 1: The boundary conditions are non-dissipation, i.e., acoustic rigid, pressure-release, and purely reactive impedance. Modes are mutual-orthogonal, i.e., $\int_s \tilde{\phi}_i \tilde{\phi}_j^* ds = 0$, left eigenfunctions $\tilde{\varphi}_n$ are equal to right eigenfunctions $\tilde{\phi}_n$. In this case, $S_{ij} = 0$ and $K_p = 1$.

Case 2: At Cremer's optimum impedances or EPs. Eigenfunctions coalesce between a pair of neighbour modes; Left and right eigenfunctions are self-orthogonal $\int_s \tilde{\phi}_n \tilde{\varphi}_n^* ds = 0$, therefore $K_p \to \infty$. In Figs. 10 and 11, we plot S_{ij} for $i = 0$ and $j = 1$, and K_p for $n = 0$ vary over the complex β_0 plane. It is shown clearly that at $\beta_{\text{Cremer}}(\beta_{\text{EP}}) = 0.099346 + 0.042653j$, $S_{01} = 1$ and $K_{p,0} = 6000$ and tend to be infinite. Varying along an arbitrary path in the complex β_0 plane, K_p and S_{ij} varies between the two opposite extremes.

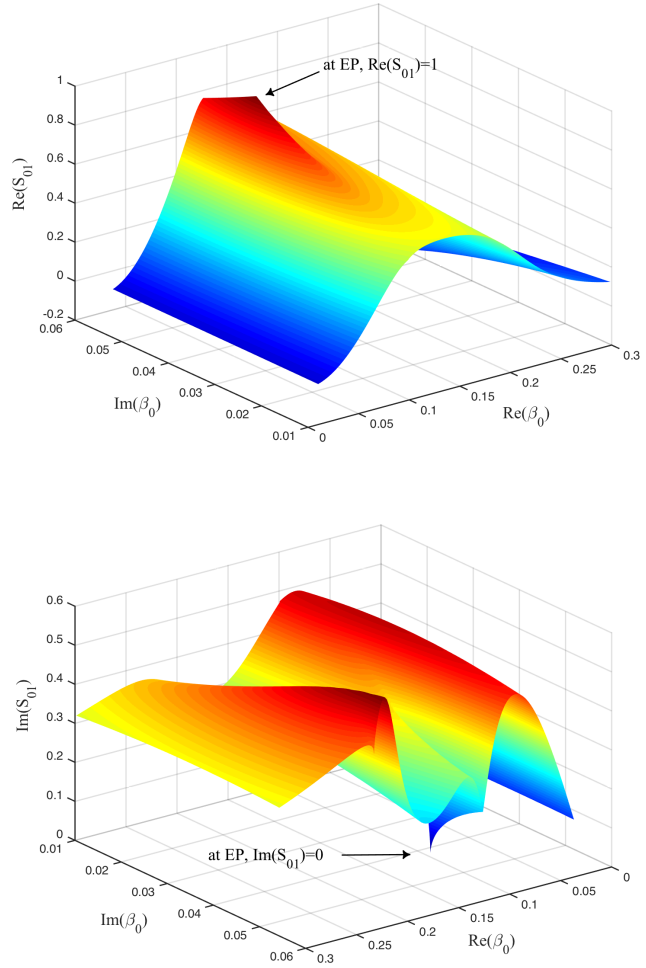

Figure 10: (Color online) Real and imaginary parts of mutual-nonorthogonality S_{01} over the complex β_0 plane. It is noted that for seeing clearly $\Im m(S_{01}) = 0$ at the first EP, we set x-axis ($\Re e(\beta_0)$) values decrease from left to right, and y-axis ($\Im m(\beta_0)$) values decrease from front to back.

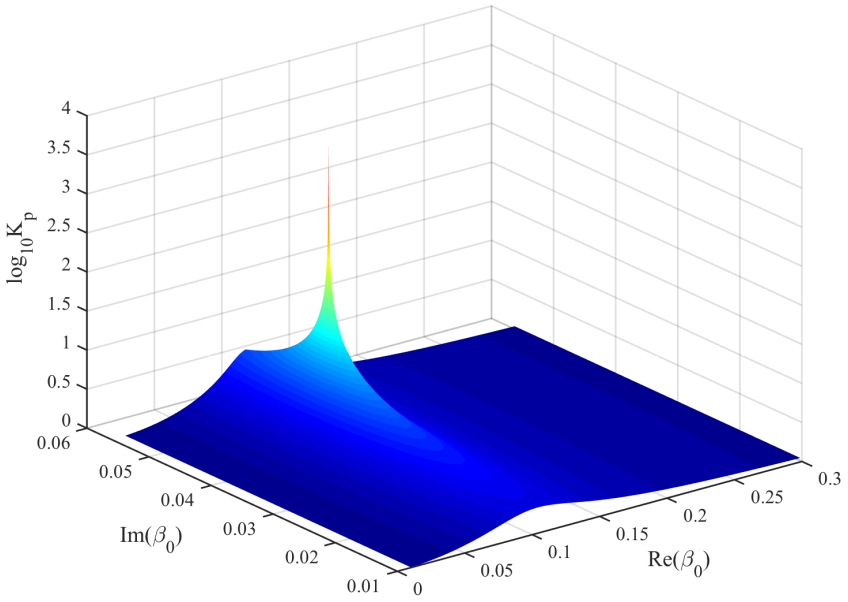

Figure 11: (Color online) Self-nonorthogonality $\log_{10}(K_p)$ over the complex β_0 plane for the first mode $n = 0$. $m = 0$.

3 Effects of K_p and S_{ij} in sound power attenuation

In this section, we will give a simple example to illustrate the important roles of K_p and S_{ij} in sound power attenuation. As shown in Fig. 12, an infinite, cylindrical waveguide with circular cross-section is considered. The left half semi-infinite wall ($z < 0$) is rigid and the right half semi-infinite wall ($z > 0$) is assumed as complex uniform impedance boundary conditions. The sound pressure satisfies the Helmholtz equation

$$\nabla_\perp^2 p + \frac{\partial^2 p}{\partial z^2} + K^2 p = 0, \tag{19}$$

where

$$\nabla_\perp^2 = \frac{1}{r}\frac{\partial}{\partial r}(r\frac{\partial}{\partial r}) + \frac{1}{r^2}\frac{\partial^2}{\partial \theta^2}, \tag{20}$$

and the boundary condition

$$\frac{\partial p}{\partial r} = Yp, \quad \text{at} \quad r = 1, \tag{21}$$

where $K = \omega R/c_0$ refers to the dimensionless wave number, $Y = -jK\beta_0$, and β_0 is the wall admittance. Pressures and lengths are respectively divided by $\rho_0 c_0^2$ and R (the duct radius) and become dimensionless variables, where ρ_0 and c_0 refer

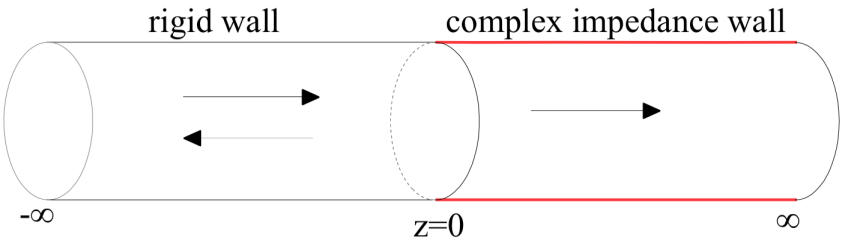

Figure 12: (Color online) Configuration of the example. The z-coordinate is aligned with the centre axis of the cylindrical waveguide. The left half semi-infinite wall ($z < 0$) is rigid and the right half semi-infinite wall ($z > 0$) is assumed as complex impedance boundary conditions.

to ambient density and speed of sound in air, respectively. Rigid muilti-modes are incident from $-\infty$. Because the wall impedance is circumferentially uniform, eigenfunctions are decoupled in the circumferential direction. Without loss of generality, we consider only circumferential mode $m = 0$.

Sound pressure in the semi-infinite WIBC is expanded over right normalized eigenfunctions $\mathbf{\Phi}(r) = [\phi_0, \phi_1, \cdots, \phi_n, \cdots, \phi_N]^T$

$$p(r, z) = \mathbf{\Phi}^T \mathsf{E}_l(z) \mathbf{C}, \tag{22}$$

where $\mathbf{C}$ is an amplitude vector of dimension N, $\mathsf{E}_l(z)$ is a diagonal matrix with $\exp(-jK_n z)$ on the main diagonal, with $K_n = \sqrt{K^2 - \gamma_n^2}$. ϕ_n and γ_n are defined in Eqs. (1, 2). "^{T}" refers to transpose. N refers to the truncation of the expansion. The eigenfunctions are normalized as defined in Eq. (11). It is noted that although there is no mathematical theorem to guarantee the completeness of ϕ_n, $n = 0 - \infty$, however, except at the infinite exceptional points, we found numerically that the expansion is convergent, in general, in the whole complex plane.

The continuities of pressure and axial particle velocity at $z = 0$ lead to

$$\mathbf{\Psi}^T(\mathbf{A} + \mathbf{B}) = \mathbf{\Phi}^T \mathbf{C}, \tag{23}$$

$$\mathbf{\Psi}^T \mathsf{K}_r(\mathbf{A} - \mathbf{B}) = \mathbf{\Phi}^T \mathsf{K}_l \mathbf{C}, \tag{24}$$

where $\mathbf{\Psi} = [\psi_0, \psi_1, \cdots, \psi_n, \cdots, \psi_N]^T$, K_r and K_l are diagonal matrices with the axial wavenumbers $\sqrt{K^2 - \alpha_n^2}$ and $\sqrt{K^2 - \gamma_n^2}$ on their main diagonal, respectively. ψ_n and α_n are the normalised eigenfunctions and eigenvalues of modes in the semi-infinite waveguide with rigid boundary conditions. $\mathbf{A}$ and $\mathbf{B}$ are the amplitude vectors of incident and reflected modes.

Projecting Eq. (23) over the left normalised eigenfunctions $\boldsymbol{\varphi}^* = [\varphi_0, \varphi_1, \cdots, \varphi_n, \cdots, \varphi_N]^{*T}$, and Eq. (24) over the normalised rigid eigenfunctions $\mathbf{\Psi}^*$, we obtain

$$\begin{aligned} \mathsf{G} &= (\mathsf{K}_r + \mathsf{F}^T \mathsf{K}_l \mathsf{K}_p' \mathsf{F})^{-1} (\mathsf{K}_r - \mathsf{F}^T \mathsf{K}_l \mathsf{K}_p' \mathsf{F}), \\ \mathbf{B} &= \mathsf{G}\mathbf{A}, \\ \mathbf{C} &= \mathsf{K}_p' \mathsf{F}(\mathsf{I} + \mathsf{G})\mathbf{A}, \end{aligned} \tag{25}$$

where

$$\mathsf{F} = \int_0^1 \boldsymbol{\varphi}^* \boldsymbol{\Psi}^T r dr, \tag{26}$$

describes the couplings between the eigenfunctions of modes in the semi-infinite waveguides of rigid wall and complex impedance wall, respectively. K'_p is a diagonal matrix with $K'_{p,n}$ defined in Eq. (17) on the main diagonal.

Sound power in the semi-infinite WIBC is

$$\begin{aligned} W &= \frac{1}{2}\Re e\{\int_0^1 p(r,\theta) v_z^*(r,\theta) r dr\} \qquad (27)\\ &= \frac{1}{2}\Re e[\mathbf{A}^T(\mathsf{I}+\mathsf{G})^T \mathsf{F}\mathsf{E}_l(z)\mathsf{K}'_p \mathsf{S}_{ij}(\mathsf{K}'_p)^*(\mathsf{K}_l/K)\mathsf{E}_l^*(z)\mathsf{F}^*(\mathsf{I}+\mathsf{G})^{*T}\mathbf{A}^*]\\ &= \underbrace{\frac{1}{2}\Re e[\sum_{i=j} |C'_i|^2 K_{p,i}\frac{K^*_{l,i}}{K} e^{-\Im m(K_{l,i})z}]}_{\text{sum of sound power in individual mode}} + \underbrace{\frac{1}{2}\Re e[\sum_{i\neq j} C'_i C'^*_j K'_{p,i} S_{ij}(K'_{p,j})^* \frac{K^*_{l,j}}{K} e^{-j(K_{l,i}-K^*_{l,j})z}]}_{\text{sum of cross power}}, \end{aligned}$$

where

$$\mathsf{C}' = \mathsf{F}(\mathsf{I}+\mathsf{G})\mathbf{A}, \tag{28}$$

is a column vector, $C'_{i(j)}$ are the elements of C', S_{ij} is a matrix, its elements S_{ij} are defined in Eq. (18), $K_{l,i(j)}$ are the elements $i(j)$ of the wavenumber matrix K_l.

Equation (27) clearly shows that the sound power are mainly decided not only by the individual mode attenuation factors $\mathsf{E}_l(z)$ (diagonal matrix with $e^{-jK_{l,i}z}$ on the main diagonal), but also by self-nonorthogonality K_p and mutual-nonorthogonality S_{ij}, and F which describes the couplings between eigenfunctions of modes in the semi-infinite waveguides of rigid wall and complex impedance wall.

In Fig. 13, we show sound power as a function of z for two two cases: Case 1, $Z = 0.1 - j$ in which the dissipation in the boundary wall is less important; Case 2, $\beta_0 = 0.0993 + 0.0427$ which is close to the first EP ($m = 0$), the boundary wall is very dissipative. Rigid multi-modes with coefficient

$$A_i = \int_0^1 \psi_i \varphi_0 r dr = \int_0^1 \psi_i \frac{1}{\sqrt{\Lambda_0}} (\frac{J_0(\gamma_0 r)}{J_0(\gamma_0)})^* r dr, \tag{29}$$

are incident, where "*" refers to complex conjugate, $i = 0 - 50$ are incident rigid mode index. J_0 is zero order Bessel function. Without loss of generality, we use $K = 30$, which is a typically industrial value in the lined intakes of an aeroengine.

For case 1, small dissipation is included, K_p are approximately equal to 1 for all modes as shown in Fig. 14 (a). Modes are approximately mutual-orthogonal. S_{ij} ($i \neq j$) are approximately equal to zero as shown in Fig. 14 (b). The total sound power and the sum of sound power in individual mode decrease exponentially, as we expect intuitively, as shown in Fig. 13 (a). The sum of cross-power is not important as shown in Fig. 13 (b). (For comparison, we plot also in Fig. 13 (b) the total sound power and the sum of sound power in individual mode. Note that

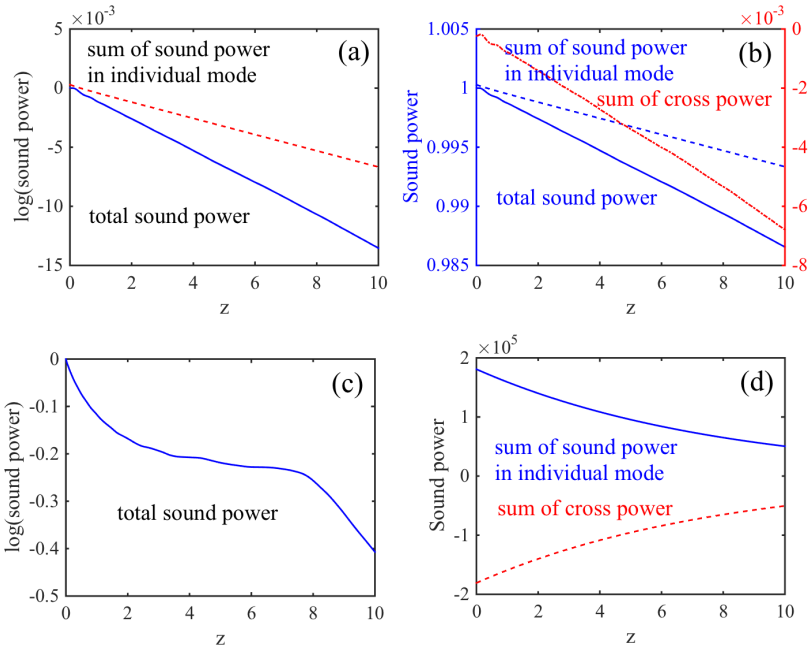

Figure 13: (Color online) Sound power as a function of z. (a) Total sound power (solid line) and sum of sound power in individual mode (dashed line) for case 1: $Z = 0.1 - j$. (Sound power is in logarithm scale.) (b) Total sound power (solid line), sum of sound power in individual mode (dashed line) and sum of cross power (dash-dot line) for case 1: $Z = 0.1 - j$. (Sound power is in linear scale.) (c) Total sound power for case 2: $\beta_0 = 0.0993 + 0.0427j$. (Sound power is in logarithm scale.) (d) Sum of sound power in individual mode (solid line) and sum of cross power for case 2: $\beta_0 = 0.0993 + 0.0427j$. (Sound power is in linear scale.) $K = 30$.

they are shown in linear scale.) This conclusion can be also obtained directly from Eq. (27).

However, for case 2 in which the impedance is close to the first EP, the acoustically absorbent material is very dissipative, it is very surprise that the total sound power attenuation curve has a plateau between about $z = 2$ and $z = 8$ where total sound power almost does not attenuate as shown in Fig. 13 (c). The sum of sound power in individual mode decreases still exponentially (not shown), but with very large amplitude (about 10^5) as shown in Fig. 13 (d). The sum of cross-power are negative and increases with z with almost the same order of amplitude. By these results, we can conclude safely that although Cremer's optimum impedances give the maximum attenuation for individual mode, however, they stimulate simultaneously very high amplitudes for the corresponding mode, the total sound power attenuation is mainly decided by the sum of sound power in individual mode and the sum of cross power cancel each other out.

This can be explained also by Eq. (27) in which the amplitudes of modes

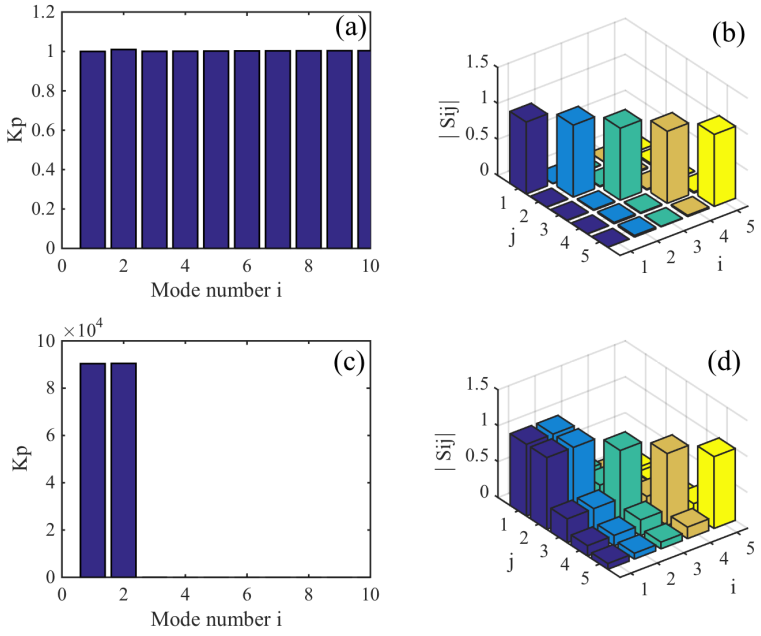

Figure 14: (Color online) Self-nonorthogonality K_p and mutual-nonorthogonality S_{ij}. (a) K_p for case 1, $Z = 0.1 - j$. (b) S_{ij} for case 1, $Z = 0.1 - j$. (c) K_p for case 2, $\beta_0 = 0.0993 + 0.0427j$. S_{ij} for case 2, $\beta_0 = 0.0993 + 0.0427j$. $K = 30$.

$i = 0$ and $j = 1$ are extremely larger than these of other modes. The two modes dominate the total sound power, the sum of sound power in individual mode, and the sum of cross power over other modes. The extremely large amplitudes are due to the nearly self-orthogonalities between left and right eigenfunctions of the almost coalescent modes $i = 0$ and $j = 1$ near the first EP. This can be seen by the K_p shown in Fig. 14 (c) whose values are approximately equal to 9×10^4 for modes $i = 0$ and $j = 1$ and are extremely larger than these of other modes. The important effects of cross-power are produced by the mutual-nonorthogonality S_{ij}. In this case, S_{01} and S_{10} are approximately equal to 1 as shown in Fig. 14 (d). Because the two modes $i = 0$ and $i = 1$ are almost coalescent, $K'_{p,0}$ and $K'_{p,1}$ are approximately equal. Similary, C'_0, K_0 are are approximately equal to C'_1 and K_1, therefore the sum of sound power in individual mode and the sum of cross power cancel each other out.

4 Conclusions

In this paper, we have given new insights into the nonorthogonalities of eigenfunctions in a waveguide with impedance boundary conditions. We have defined two quantities: self-nonorthogonality Kp, which measures the nonorthogonality between left and right eigenfunctions of a mode, and mutual-nonorthogonality

S_{ij}, which measures the nonorthogonality between modes i and j. Two opposite limiting cases are clearly identified in the complex boundary admittance β_0 plane. One is non-dissipation, i.e., acoustic rigid, pressure-release, and purely reactive impedance. Modes are mutual-orthogonal. Left eigenfunctions are equal to right eigenfunctions. $S_{ij} = 0$ and $K_p = 1$. The other is Cremer's optimum impedances which are exceptional points. Both eigenvalues and eigenfunctions coalesce between a pair of neighbour modes i and j. Left and right eigenfunctions of the coalescent modes are self-orthogonal. In this case, $S_{ij} = 1$ and $K_p = \infty$.

The total sound power in the waveguide is mainly decided by K_p, S_{ij}, besides the exponential attenuation factors $e^{-jK_l z}$. We have shown that although Cremer's optimum impedances give the maximum attenuation for individual mode, however, they simultaneously stimulate very high amplitudes for the corresponding mode. When the acoustically absorbent materials are very dissipative, the total sound power attenuation is mainly decided by the cancel each other out between the sum of sound power in individual mode and the sum of cross power.

A Adjoint eigenvalue problem and bi-orthogonal relation

We consider an operator $\mathscr{L} = \nabla_\perp^2 + \gamma_{mn}^2$, the eigenvalue problem defined by Eqs. (1) and (2) can be rewritten as

$$\mathscr{L}\tilde{\phi}_{mn} = 0, \tag{30}$$

with the boundary condition

$$\mathscr{G}\tilde{\phi}_{mn} = 0, \text{ at } r = 1, \tag{31}$$

where $\mathscr{G} = \partial/\partial r - Y$. By introducing a function $\tilde{\varphi}$ which satisfies

$$\int_s \tilde{\varphi}^*_{m'n'} \mathscr{L}\tilde{\phi}_{mn} ds = \int_s \tilde{\varphi}^*_{m'n'} (\nabla_\perp^2 + \gamma_{mn}^2)\tilde{\phi}_{mn} ds \tag{32}$$

$$= \int_s \tilde{\phi}_{mn} [\nabla_\perp^2 + \gamma_{mn}^2]\tilde{\varphi}^*_{m'n'} ds + \oint \left(\tilde{\varphi}^*_{m'n'} \frac{\partial \tilde{\phi}_{mn}}{\partial r} - \tilde{\phi}_{mn} \frac{\partial \tilde{\varphi}^*_{m'n'}}{\partial r} \right) dC \tag{33}$$

$$= \int_s (\mathscr{L}^+ \tilde{\varphi}_{m'n'})^* \tilde{\phi}_{mn} ds - \int_0^{2\pi} \tilde{\phi}_{mn} \left(\frac{\partial \tilde{\varphi}^*_{m'n'}}{\partial r} - Y\tilde{\varphi}^*_{m'n'} \right) d\theta$$

$$= \int_s (\mathscr{L}^+ \tilde{\varphi}_{m'n'})^* \tilde{\phi}_{mn} ds - \int_0^{2\pi} \tilde{\phi}_{mn} (\mathscr{G}^+ \tilde{\varphi}_{m'n'})^*,$$

where

$$\mathscr{L}^+ = \nabla_\perp^2 + (\gamma_{mn}^2)^* = \nabla_\perp^2 + \epsilon_{m'n'}^2, \quad \mathscr{G}^+ = \partial/\partial r - Y^*, \tag{34}$$

we can define the adjoint eigenvalue problem as

$$\mathscr{L}^{+}\tilde{\varphi}_{m'n'} = 0, \tag{35}$$

with the boundary condition

$$\mathscr{G}^{+}\tilde{\varphi}_{m'n'} = 0, \text{ at } r = 1. \tag{36}$$

Multiplying Eq. (30) by $\tilde{\varphi}^{*}_{m'n'}$ and the conjugate of Eq. (35) by $\tilde{\phi}_{mn}$ for different mode $\gamma^2_{mn} \neq (\epsilon^2_{m'n'})^{*}$, i.e., $m \neq m'$ and $n \neq n'$, and subtracting the results, we obtain

$$\begin{aligned}
[\gamma^2_{mn} - (\epsilon^2_{m'n'})^{*}] \int_s \tilde{\phi}_{mn}\tilde{\varphi}^{*}_{m'n'} ds &= \int_s (\tilde{\phi}_{mn}\nabla^2_{\perp}\tilde{\varphi}^{*}_{m'n'} - \tilde{\varphi}^{*}_{m'n'}\nabla^2_{\perp}\tilde{\phi}_{mn}) ds && (37)\\
&= \oint \left(\tilde{\phi}_{mn}\frac{\partial \tilde{\varphi}^{*}_{m'n'}}{\partial r} - \tilde{\varphi}^{*}_{m'n'}\frac{\partial \tilde{\phi}_{mn}}{\partial r} \right) dC && (38)\\
&= \int_0^{2\pi} \tilde{\phi}_{mn} \left(\frac{\partial \tilde{\varphi}^{*}_{m'n'}}{\partial r} - Y\tilde{\varphi}^{*}_{m'n'} \right) d\theta \\
&= 0,
\end{aligned}$$

where we have used Eq. (36), $\mathscr{G}^{+}\tilde{\varphi}_{mn} = 0$. Therefore,

$$\int_s \tilde{\phi}_{mn}\tilde{\varphi}^{*}_{m'n'} ds = 0, \quad \text{when } m \neq m',\ n \neq n'. \tag{39}$$

When the boundary is acoustically rigid ($Y = 0$), pressure release ($Z = 0$), or purely reactive without dissipation ($\beta_0 = jc$, $Y = -jK\beta_0 = Kc$, c is real),

$$\mathscr{L}^{+} = \mathscr{L}, \ \ \mathscr{G}^{+} = \mathscr{G}, \tag{40}$$

the eigenvalue problem defined by Eqs. (1) and (2) or (30) and (31) is self-adjoint. It is easy to show that γ^2_{mn} are real and $\tilde{\varphi}_{mn} = \tilde{\phi}_{mn}$.

On the other hand, for all practical problem, β_0 and therefore Y are complex. Taking the complex conjugate of Eqs. (35) and (36), we obtain

$$\tilde{\varphi}_{mn} = \tilde{\phi}^{*}_{mn}. \tag{41}$$

The orthogonal relation (39) is then rewritten as the bi-orthogonality (10)

$$\int_s \tilde{\phi}_{mn}\tilde{\varphi}^{*}_{m'n'} ds = \int_s \tilde{\phi}_{mn}\tilde{\phi}_{m'n'} ds = 0, \quad \text{when } m \neq m',\ n \neq n'. \tag{42}$$

B Branch point on the complex admittance plane

We consider the variation of eigenvalues as a function of complex admittance. At some admittances, the eigenvalues of a pair of neighbour modes coalesce to form

Branch Points (BP) on the complex admittance plane. At the BP, the dispersion equation (4) has double eigenvalues $\gamma_{\rm BP}$, i.e.

$$\gamma_{m_0 n}\frac{J'_{m_0}(\gamma_{m_0 n})}{J_{m_0}(\gamma_{m_0 n})}\Big|_{\gamma_{m_0 n}=\gamma_{\rm BP}} = -jK\beta_{\rm BP}, \tag{43}$$

$$\frac{\partial}{\partial\gamma_{m_0 n}}\left(\gamma_{m_0 n}\frac{J'_{m_0}(\gamma_{m_0 n})}{J_{m_0}(\gamma_{m_0 n})}\right)\Big|_{\gamma_{m_0 n}=\gamma_{\rm BP}} = 0, \tag{44}$$

where we have fixed $m = m_0$, $\gamma_{m_0 n}$ are eigenvalues, J_{m_0} are the m_0 order Bessel function, the prime refers to derivative with respect to $\gamma_{m_0 n}$. K is dimensionless frequency. If we define a function

$$f(\gamma_{m_0 n},\beta_0) = \gamma_{m_0 n}\frac{J'_{m_0}(\gamma_{m_0 n})}{J_{m_0}(\gamma_{m_0 n})} + jK\beta_0, \tag{45}$$

we expand the function $f(\gamma_{m_0 n},\beta_0)$ in the vicinity of $(\gamma_{\rm BP},\beta_{\rm BP})$ to the lowest order as

$$f(\gamma_{m_0 n},\beta_0) \approx \frac{1}{2}\frac{\partial^2 f}{\partial\gamma_{m_0 n}^2}\Big|_{\gamma_{m_0 n}=\gamma_{\rm BP}}(\gamma_{m_0 n}-\gamma_{\rm BP})^2 + \frac{\partial f}{\partial\beta_0}\Big|_{\beta_0=\beta_{\rm BP}}(\beta_0-\beta_{\rm BP}). \tag{46}$$

Suppose that in the vicinity of $(\gamma_{\rm BP},\beta_{\rm BP})$, $\partial^2 f/\partial\gamma_{m_0 n}^2 \neq 0$, i.e. there has no triple or higher order eigenvalues of dispersion equation (4), we obtain,

$$\gamma_{m_0 n}-\gamma_{\rm BP} \approx -\sqrt{\frac{2\partial f/\partial\beta_0}{\partial^2 f/\partial\gamma_{m_0 n}^2}}\sqrt{\beta_0-\beta_{\rm BP}}. \tag{47}$$

$\beta_{\rm BP}$ is a square root branch point in the complex admittance plane.

References

[1] A. D. Pierce, *Acoustics, An introduction to its physical principles and applications* (McGraw-Hill Book Company, New York, 1981), Chap. VII.

[2] P. M. Morse and K. U. Ingard, *Theoretical acoustics* (McGraw-Hill Book Company, New York, 1968), Chap. IX.

[3] A. H. Nayfeh, J. E. Kaiser and D. P. Telionis, "Acoustics of aircraft engine-duct systems," AIAA J. **13**, 130-153 (1975).

[4] L. Cremer, "Theory of sound attenuation in a rectangular duct with an absorbing wall and the resultant maximum attenuation coefficient," (in german) Acustica **2**, 249-263 (1953).

[5] B. J. Tester, "The optimization of modal sound attenuation in duct, in the absence of mean flow," J. Sound Vib. **27**, 477-513 (1973).

[6] W. E. Zorumski and J. P. Mason, "Multiple eigenvalues of sound-absorbing circular and annular ducts," J. Acoust. Soc. Am. **55**, 1158-1165 (1974).

[7] W. Eversman, *Theoretical models for duct acoustic propagation and radiation*, in *Aeroacoustics of flight vehicles: theory and practice. Volume 2: noise control*, AD-A241, 142 (1991), Chap. XIII.

[8] F. P. Mechel, "Modal solutions in rectangular ducts lined with locally reacting absorbers," Acustica **73**, 223-239 (1991).

[9] F. P. Mechel, "Modal solutions in circular and annular ducts with locally or bulk reacting lining," Acustica **84**, 201-222 (1998).

[10] W. Koch, "Attenuation of sound in multi-element acoustically lined rectangular ducts in the absence of mean flow," J. Sound Vib. **52**, 459-496, (1977).

[11] E. J. Rice, "Multimodal far-field acoustic radiation pattern using mode cutoff ratio," AIAA J. **16**, 906-911 (1978).

[12] E. J. Rice, "Optimum wall impedance for spinning modes - a correlation with mode cut-off ratio," J. Aircraft **16**, 336-343 (1979).

[13] L. J. Heidelberg and E. J. Rice, "Experimental evaluation of a spinning-mode acoustic treatment," NASA-1613 (1980).

[14] W. Eversman, "Effect of lining non-linearity on realized attenuation of tonal noise," Procedia Engineering **6**, 114-123 (2010).

[15] W. R. Watson, "Circumferentially segmnted duct liners optimized for axisymmetric and standind-wave sources," NASA-2075 (1982).

[16] W. R. Watson, M. G. Jones, T. L. Parrott, and J. Sobieski, "Assessment of equation solvers and optimization techniques for nonaxisymmetric liners," AIAA J. **42**, 2010-2018 (2004).

[17] L. M. B. C. Campos and J. M. G. S. Oliveira, "On the acoustic modes in a cylindrical duct with an arbitrary wall impedance distribution," J. Acoust. Soc. Am. **116**, 3336-3347 (2004).

[18] G. W. Bielak, J. W. Premo and A. S. Hersh, "Advanced turbofan duct liner concepts," NASA/CR-1999-209002 (1999).

[19] P. M. Morse, "The transmission of sond pipes," J. Acoust. Soc. Am. **11**, 205-210 (1939).

[20] E. L. Shenderov, "Helmholtz equation solutions corresponding to multiple roots of the dispersion equation for a waveguide with impedance walls," Acoustical Physics **46**, 357-363 (2000).

[21] S. W. Rienstra, "A classification of duct modes based on surface waves," Wave Motion **37**, 119-135 (2003).

[22] C. Dembowski, H. D. Graf, H. L. Harney, A. Heine, W. D. Heiss, H. Rehfeld, and A. Richter, "Experimental observation of the topological structure of exceptional points," Phys. Rev. Lett. **86**, 787 (2001).

[23] W. D. Heiss and A. L. Sannino, "Avoided level crossing and exceptional points," J. Phys. A: Math. Gen. **23**, 1167-1178 (1990).

[24] W. D. Heiss and A. L. Sannino, "Transitional regions of finite Fermi systems and quantum chaos," Phys. Rev. A **43**, 4159-4166 (1991).

[25] W. D. Heiss, "Exceptional points of non-Hermitian operators," J. Phys. A: Math. Gen. **37**, 2455-2464 (2004).

[26] W. D. Heiss, "The physics of exceptional points," J. Phys. A: Math. Theor. **45**, 444016 (2012).

[27] I. Rotter, "A non-Hermitian Hamilton operator and the physics of open quantum systems," J. Phys. A: Math. Theor. **42**, 153001 (2009).

[28] M. V. Berry, "Physics of nonhermitian degeneracies," Czechoslovak J. of Phys. **54**, 1039-1047 (2004).

[29] O. Latinne, N. J. Kylstra, M. Drr, J. Purvis, M. Terao-Dunseath, C. J. Joachain, P. G. Burke, and C. J. Noble, "Laser-induced degeneracies involving autoionizing states in complex atoms," Phys. Rev. Lett. **74**, 46 (1995).

[30] T. Stehmann, W. D. Heiss and F. G. Scholtz, "Observation of exceptional points in electronic circuits," J. Phys. A **37**, 7813 (2004).

[31] H. Cartarius, J. Main, and G. Wunner, "Exceptional points in atomic spectra," Phys. Rev. Lett. **99**, 173003 (2007).

[32] S. B. Lee, J. Yang, S. Moon, S-Y Lee, J-B Shim, S. W. Kim, J-H Lee, and K. An, "Observation of an exceptional point in a chaotic optical microcavity," Phys. Rev. Lett. **103**, 134101 (2009).

[33] S. Klaiman, U. Günther, and N. Moiseyev, "Visualization of branch points in PT-symmetric waveguides," Phys. Rev. Lett. **101**, 080402 (2008).

[34] W. P. Bi and V. Pagneux, "Resonance trapping in waveguides with impedance boundary conditions," to be submitted.

[35] A. W. Leissa, "On a curve veering aberration," J. Applied Math. and Phys. (ZAMP) **25**, 99-111 (1974).

[36] J. R. Kuttler and V. G. Sigillito, "On curve veering," J. Sound and Vib. **75**, 585-588 (1981).

[37] C. H. Hodges, "Confinement of vibration by structural irregularity," J. Sound Vib. **82**, 441-424 (1982).

[38] C. H. Hodges and J. Woodhouse, "Vibration isolation from irregularity in a nearly periodic structure: theory and measurements," J. Acoust. Soc. Am. **74**, 894-905 (1983).

[39] C. Pierre and E. H. Dowell, "Localization of vibrations by structural irregularity," J. Sound Vib. **114**, 549-564 (1987).

[40] C. Pierre, "Mode localization and eigenvalue loci veering phenomena in disordered structures," J. Sound Vib. **126**, 485-502 (1988).

[41] M. S. Triantafyllou and G. S. Triantafyllou, "Frequency coalescence and mode localization phenomena: a geometric theory," J. Sound Vib. **150**, 485-500 (1991).

[42] K. Petermann, "Calculated spontaneous emission factor for double-heterostructure injection lasers with gain-induced waveguiding," IEEE J. Quantum Electron. **QE-15** 566 (1979).